SPE-218872-MS

Numerical Investigation of CO_2 Convective Transport in Stochastically Generated Heterogenous Media: Implications for Long-Term CO_2 Sequestration in Saline Aquifers

Md Fahim Shahriar and Aaditya Khanal, Jasper Department of Chemical Engineering, University of Texas at Tyler, Tyler, TX, USA

This paper was prepared for presentation at the SPE Western Regional Meeting held in Palo Alto, California, USA, 16 - 18 April 2024.

Abstract

Dissolution trapping is one of the most dominant mechanisms for CO_2 storage in subsurface porous media saturated with brine. The CO_2 dissolution rate and overall fluid flow dynamics in subsurface formations can vary significantly based on permeability variation. Although some numerical simulations have focused on these factors, detailed flow behavior analysis under nonuniform permeability distribution needs further study. For this purpose, we conduct simulations on the flow behavior of CO_2-dissolved brine in two different heterogeneous media. The spatial permeability variations in the cell enable the analysis of complex subsurface storage phenomena, such as changes in finger morphology and preferential dissolution path. Finally, the amount of CO_2 dissolved was compared between each case, based on which we draw informed conclusions about CO_2 storage sites. The results demonstrated a preferential movement of CO_2-dissolved regions toward high permeability regions, whereas a poor sweep efficiency was observed due to minimum dissolution in areas with lower permeability. Furthermore, simulation results also reveal uneven CO_2 concentration inside the convective fingers. This study provides fundamental insight into the change in flow behavior at heterogeneous regions, which could be translated into saline aquifer conditions. The proposed workflow in this study could be extended further to analyze complex heterogeneous storage systems at different flow regimes.

Keywords: CO_2 Sequestration, Dissolution Trapping, Relative Permeability Hysteresis, Capillary pressure, Diffusion

Introduction

The atmospheric concentration of CO_2 increased by almost 50% compared to the beginning of the industrial revolution, causing irreversible damage to ecosystems (Aldred et al., 2021). The effects of rising surface temperatures due to increased CO_2 emissions are also evident from frequent natural disasters, which are reported to have caused around \$2.28 trillion in losses from 1980 (Shahriar & Khanal, 2023b). Recent studies have focused on CO_2 capture and storage technologies to achieve environmental sustainability through CO_2 mitigations. One of the most promising ways to reduce the harmful effects of rising CO_2 concentrations is subsurface sequestration in saline aquifers, a major geological storage option because of the huge storage potential and wide availability (Shahriar & Khanal, 2023b). CO_2 is stored in saline aquifers through four trapping mechanisms: structural trapping, residual trapping, dissolution trapping, and trapping through mineralization. As observed in previous studies, dissolution trapping is the primary trapping mechanism in saline aquifers, where almost two-thirds of the injected CO_2 is stored through dissolution in brine (Khanal & Shahriar, 2022; Khosrokhavar et al., 2014).

Several experimental works have tried to unearth the fundamental aspects of dissolution trapping in saline aquifers using a Hele-Shaw cell, an apparatus built with two transparent plates with a small gap width between them (Faisal et al., 2015; Taheri et al., 2017). Using the Hele-Shaw, it is possible to visualize fluid flow on a 2D scale, including density-driven CO_2 transport, i.e., dissolution trapping. Furthermore, by varying the gap width and packing the Hele-Shaw cell with glass beads or strips with different thicknesses, different permeability and porosity conditions are obtainable, mimicking transport mechanisms for different saline aquifers (W. S. Amarasinghe et al., 2021; De et al., 2022; De Paoli et al., 2020; Singh et al., 2019). (Taheri et al., 2017) performed qualitative and quantitative tests to explore the density-driven natural convection during CO_2 storage under various conditions and different apertures and dipping angles. The objective parameters of their study were the onset time of convection, convective finger morphology, and dissolution flux of CO_2 in water. Dissolution of CO_2 under high pressure (1.5 to 5 bar) using Hele-Shaw cells was investigated in the work of (Outeda et al., 2014), where it was observed that higher pressure conditions increase the CO_2 mass influx, thus promoting faster subsurface CO_2 transport. Another study at high-pressure conditions by (Mahmoodpour et al., 2019) at around 36.9 bar reported similar findings, stating that CO_2 sequestration is favorable at high-pressure, high-temperature (HPHT) conditions. Several studies also investigated the effects of heterogeneity in subsurface CO_2 storage using Hele-Shaw cells. Amidst different forms of heterogeneities present in porous media, such as chemical heterogeneity (change in mineralogical properties), petrophysical heterogeneity (permeability and porosity variation), and biological heterogeneity (biofilm growth), petrophysical-heterogeneities have a significant effect in dictating the dissolution pattern during CO_2 subsurface aquifer storage. Therefore, most studies have considered changes in permeability or porosity while conducting experiments or numerical simulations. For example, (W. Amarasinghe et al., 2020) conducted CO_2 dissolution experiments at 100 bar and 50 °C in a Hele-Shaw cell using glass bead size of 50 to 600 μm. They observed piston-like displacement in lower permeability cases, while finger shape patterns are visible in high permeability cases. Furthermore, a preferential fingering of CO_2-rich high-density water towards the highly permeable regions was observed. Similar findings were reported in the work of (Vosper et al., 2014) using glass beads with diameters of 0.4–0.6 mm. Meanwhile, a different way of changing permeability through the Hele-Shaw cell was implemented in our previous work (Shahriar & Khanal, 2023b), where, by changing the placement of sidewall shims, we got a complex permeability distribution inside the Hele-Shaw cell. It was observed that there is a preferential finger pathway towards the high permeability regions, translating to an uneven CO_2 dissolution profile in heterogeneous media.

Various studies have also considered numerical simulations to report CO_2 dissolution behavior in subsurface porous media; however, despite the more realistic nature of heterogeneous media during CO_2 sequestration operations, most simulation studies on CO_2 dissolution in saline aquifers use homogeneous models (Alipour et al., 2020; Taheri et al., 2017; Zhang et al., 2020). The effects of heterogeneity were numerically simulated by (Soltanian et al., 2017), where the facies spatial organization was reported to be a dictating parameter for CO_2 convective dissolution. Moreover, (Wang et al., 2023) reported a deteriorated CO_2 sequestration efficiency for reservoirs with a high degree of heterogeneity. Although these studies have considered the effects of heterogeneity, a comparative analysis of the CO_2 dissolution behavior between homogeneous and heterogeneous media (different heterogeneous distributions while keeping the same average permeability) needs further study. To address this issue, we report the CO_2 dissolution between one homogeneous and two heterogeneous media with different permeability distributions. Moreover, in order to provide a comparative evaluation, we keep the average permeability of the three cases the same, allowing us to highlight only the effects of different heterogeneity formations. The remainder of the paper is organized as follows: First, we describe the governing equations, initial and boundary conditions, and solution method. Subsequently, we validate the numerical simulation model by matching the simulation results at different times to experimental results from a homogeneous model. Following this, we use the validated model to simulate two types of heterogeneous media to understand the dissolution profile. Furthermore, we compare the results to the homogeneous model to further explain the effects of permeability variation in 2D heterogeneous systems and discuss possible future studies. Finally, we present the main conclusions from this study.

Numerical Method

Governing Equations

The fluid inside the Hele-Shaw cell can be considered as continuum and incompressible under the experimental conditions (presented in Table 1); therefore, the Navier-Stokes equation and continuity were used to numerically simulate the fluid dynamics and mass transfer inside the cell (Chevalier et al., 2015; Faisal et al., 2015). The incompressible approximation is valid only because the density change of water with dissolved CO_2 is relatively small compared to the initial reference density(Emami-Meybodi et al., 2015). Therefore, the global formulation of the conservative equation for a porous media with CO_2 (gas phase, g) and water (liquid phase, l) is expressed in Eq. 1:

$$\frac{\partial}{\partial t}\left[\sum_{\gamma=l,g}\left(\phi\rho_\gamma S_\gamma \omega_\gamma^i\right)\right] = -\sum_{\gamma=l,g}\nabla\left(\rho_\gamma V_\gamma \omega_\gamma^i\right) - \sum_{\gamma=l,g}\nabla\left(J_\gamma^i\right) + \sum_{\gamma=l,g}\nabla\left(m_{d\gamma}\omega_\gamma^i\right) \quad (1)$$

Where, γ and i represent the phase (liquid or gas) and species (CO_2 or H_2O), respectively. Furthermore, ρ,ϕ,S,ω, and m_d are the density, porosity, saturation, mass fraction, and mass rate density, respectively. Boussinesq approximation is used for density calculations as the fluid properties are independent of the solute concentration at small CO_2 content in water. Furthermore, thermal effects caused by CO_2 absorption are negligible and can be ignored. A similar approach has been used in the numerical investigation of Zhang et al. (Zhang et al., 2020). The diffusive-convection process of CO_2 dissolution in water can be explained by the nonlinear governing equations as follows (Eq. 2–4):

$$\nabla . v = 0 \quad (2)$$

$$\frac{\partial \rho}{\partial t} + \nabla(\rho . v . v) = -\nabla P + \mu \nabla^2 v + F \quad (3)$$

$$\frac{\partial C_A}{\partial t} + v \nabla C_g = D_{CO_2} \nabla^2 C_g \quad (4)$$

Where, ρ, P, C_g, μ and D_{CO_2} represents the density, pressure, CO_2 concentration, viscosity, and diffusion coefficient of CO_2 in water. The liquid velocity is represented by V, and the buoyancy source in the gravity direction, represented by F, is given by:

$$F = \rho_o\left(1 + \beta_g + C_g\right)g \quad (5)$$

Where, β_g represents the solutal expansion coefficient of CO_2, and g is the gravitational acceleration.

Table 1—Physical model and the experimental conditions considered for the simulation model.

Physical Model (Graphical Illustration)	Experimental Conditions and Fluid Properties	
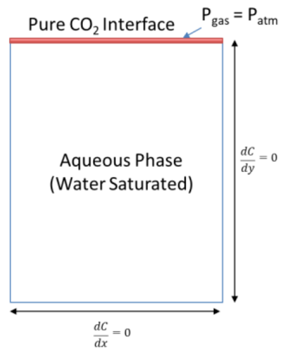	Dimensions	259 mm (width) and 242 mm (height)
	Temperature	22 °C
	Pressure	1 atm
	Salinity	No salinity
	Aperture[a]	1 mm
	Water dynamic Viscosity	0.95475×10^{-3} Pa s
	Density Variation[b]	0.29 kg/m^3
	Diffusion coefficient of CO_2 in water	1.4424×10^{-9} m^2/s

[a]Considered only for the homogeneous base case, [b]Density difference between water saturated with CO_2 (higher) and pure water (lower)

Initial and Boundary Conditions

This study's physical model (base case) is built similarly to our previous experimental configuration (Shahriar & Khanal, 2023a). The flow domain is at 22 °C and 1 atm. As shown in Table 1, the bottom and lateral boundaries have no-flow conditions, whereas the top boundary was set as a pure CO_2 interface.

Solution Method

With Ansys Fluent multiphysics software, the governing equations with initial and boundary conditions were numerically solved using the finite volume methodology. The pressure-correction method was used through the implicit iterative scheme SIMPLE algorithm, a transient algorithm commonly used for solving governing equations for density-driven convective flow (Ferziger et al., 2020; Soboleva, 2018; Zhang et al., 2020). We also selected a small time step of 0.1s, corresponding to the Newton-Raphson convergence criterion equal to 10^{-6} (Faisal et al., 2015). Pressure discretization was performed by the pressure staggering option (PRESTO), whereas quadratic upstream interpolation for convection dynamics (QUICK) was used to discretize CO_2 components and the momentum term.

Additionally, in order to induce the convection phenomenon or the fingering pattern during the CO_2 dissolution, we chose to include small sinusoidal perturbations), in the initial condition (at time $t \le 0.1$ sec) instead of using numerical rounding errors to trigger the instabilities, i.e., (Farajzadeh et al., 2011; Zhang et al., 2020).

$$c = 1 + 0.01 sin\left(2\pi x / \lambda\right) \tag{6}$$

Where, c represents the dimensionless concentration, $\lambda = \frac{1}{12}$, and x specifies the horizontal direction, following the work of Farajzadeh et al. (Farajzadeh et al., 2011). The perturbations were located at the top interface where the saturation of dissolved CO_2 is 1, similar to the work of Faisal et al. (Faisal et al., 2015). In real-life scenarios, the convection phenomenon is due to thermodynamic instabilities or other forms of heterogeneities (Farajzadeh et al., 2008; Kneafsey & Pruess, 2010).

Validation of Simulation with Experimental Results

The operating conditions for the base case simulation were set to be the same as our previous experimental work (Shahriar & Khanal, 2023a). We validate the simulation results by qualitatively comparing the CO_2 finger morphology at different timescales, as shown in Fig. 1. For similar conditions and times, the simulation results are in good agreement with the experimental finger morphology. Furthermore, the overall CO_2 dissolution behavior is observed to be similar, where at the initial stage, diffusion is the primary mass transfer mechanism, and the diffusive layer moves downward vertically without any instability or deformation. However, throughout time, the density difference between the CO_2-dissolved water and the freshwater leads to a density-driven convective flow, which is evident through the formation of small fingers.

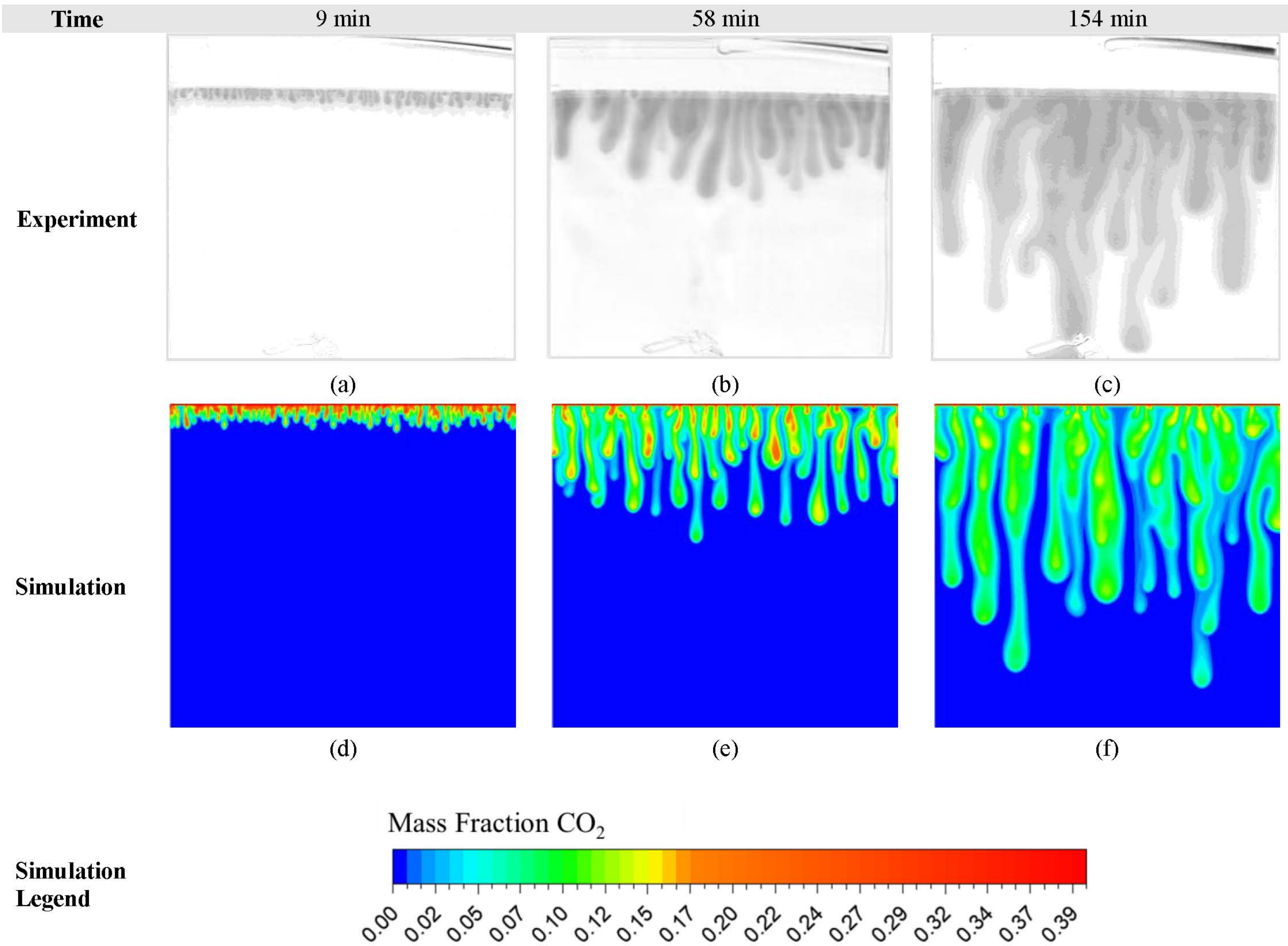

Figure 1—Validation of simulation results (d-f) with experimental results (a-c) at similar conditions for different timescales in the same order.

Furthermore, Fig. 1 shows that CO_2-dissolved fingers merge and grow in width throughout time, a phenomenon accurately portrayed in the simulations. Additionally, due to cell-scale convection, i.e., CO_2 dissolved water at the top getting replaced by the freshwater due to convective flow, nascent fingers form at the top of the gas-water interface, which is better visible through the simulation results. The simulation results also reveal uneven CO_2 concentration inside the convective fingers, which has also been reported in previous studies (Shahriar & Khanal, 2023b; Zhang et al., 2020). Another factor worth noting is the slight discrepancy in the CO_2 finger morphology and vertical travel for the experimental and simulation results. This can be attributed to the fact that the Hele-Shaw cell aperture is not perfectly homogeneous for experimental studies due to the precision of the plexiglass used. Furthermore, it should be noted that several studies also report some minor dissimilarities in convective finger morphology while performing repeatability tests (Faisal et al., 2015; Shahriar & Khanal, 2023b). Nevertheless, similar CO_2 dissolution behavior and comparable finger travel between the results ensure the validity of the simulation.

Methodology and Results of Heterogeneous Cases

Methodology for Creating Heterogeneous Regions

This study considers two heterogeneous cases 1 and 2, with different permeability variations but the same mean permeability. The mean permeability (k) of the heterogeneous cases is set to be 8.33×10^{-8} m^2, similar to the homogeneous case presented in **Section 3,** corresponding to a Hele-Shaw cell aperture (b) of 0.001 m, calculated as follows.

$$k = \frac{b^2}{12} \tag{7}$$

Sixteen different regions are created within the domain, assigning different permeability values corresponding to Hele-Shaw aperture of 0.0013, 0.0012, 0.0011, 0.0009, 0.0008, and 0.0007 m to the regions, as shown in the permeability profile in Fig. 2 and 3. In heterogeneity case 1, the permeability profile is set so that a high permeability region follows a low permeability region, and so on. In case 2, the low permeability regions are set together, allowing better connectivity between the high permeability regions. It should be noted that while the permeability distribution is different between the two cases, the mean permeability is the same, thus allowing us to specifically highlight only the effects of permeability distribution in heterogeneous media. A similar methodology is adopted in the work of (Mahyapour et al., 2022), where they considered heterogeneous media with permeability of 200 mD and 400 mD.

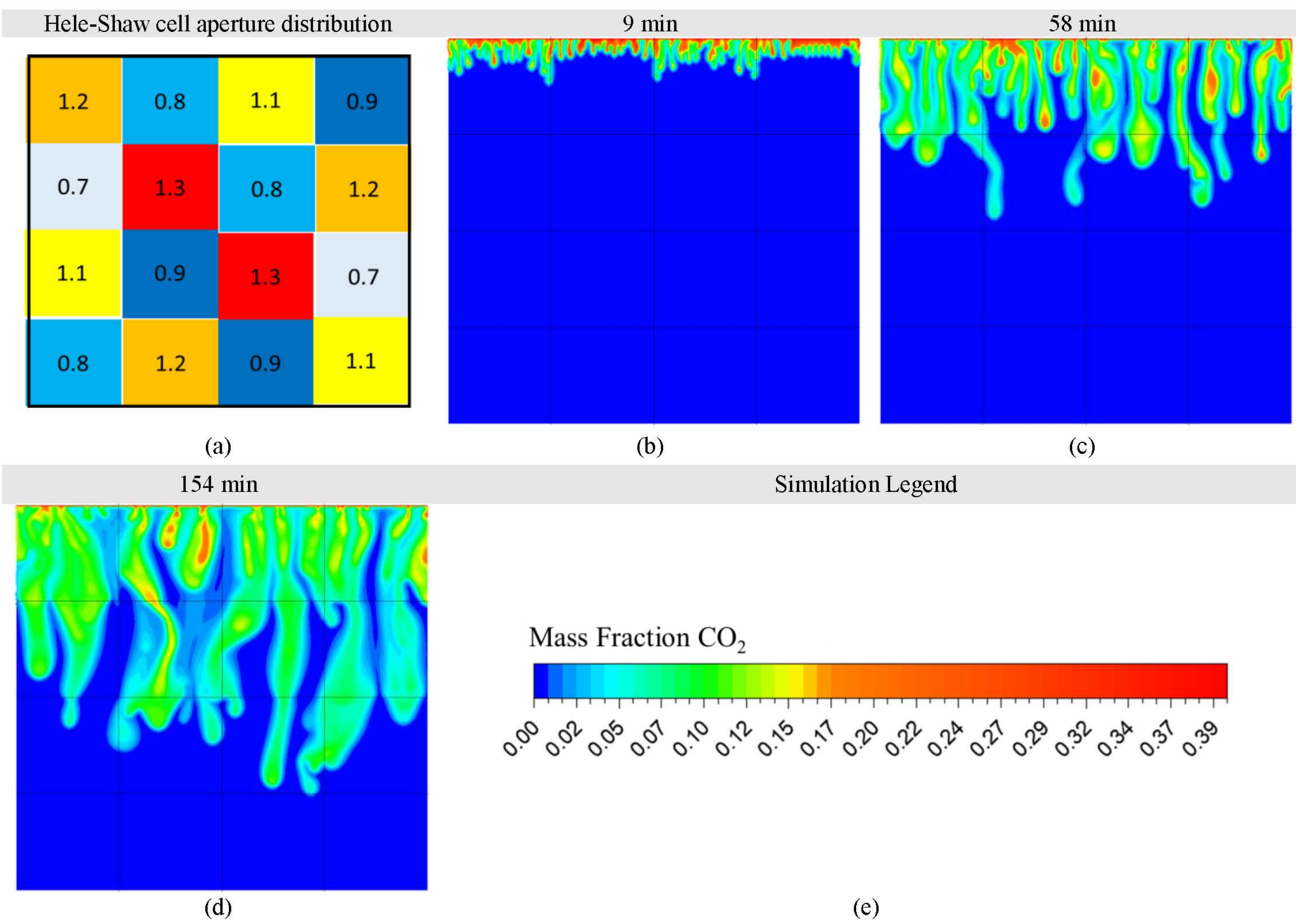

Figure 2—(a) Hele-Shaw cell aperture distribution (expressed in millimeters) and (b-d) the evolution of CO_2 dissolution through time for heterogeneous Case 1. The mass fraction of CO_2 is shown in (e).

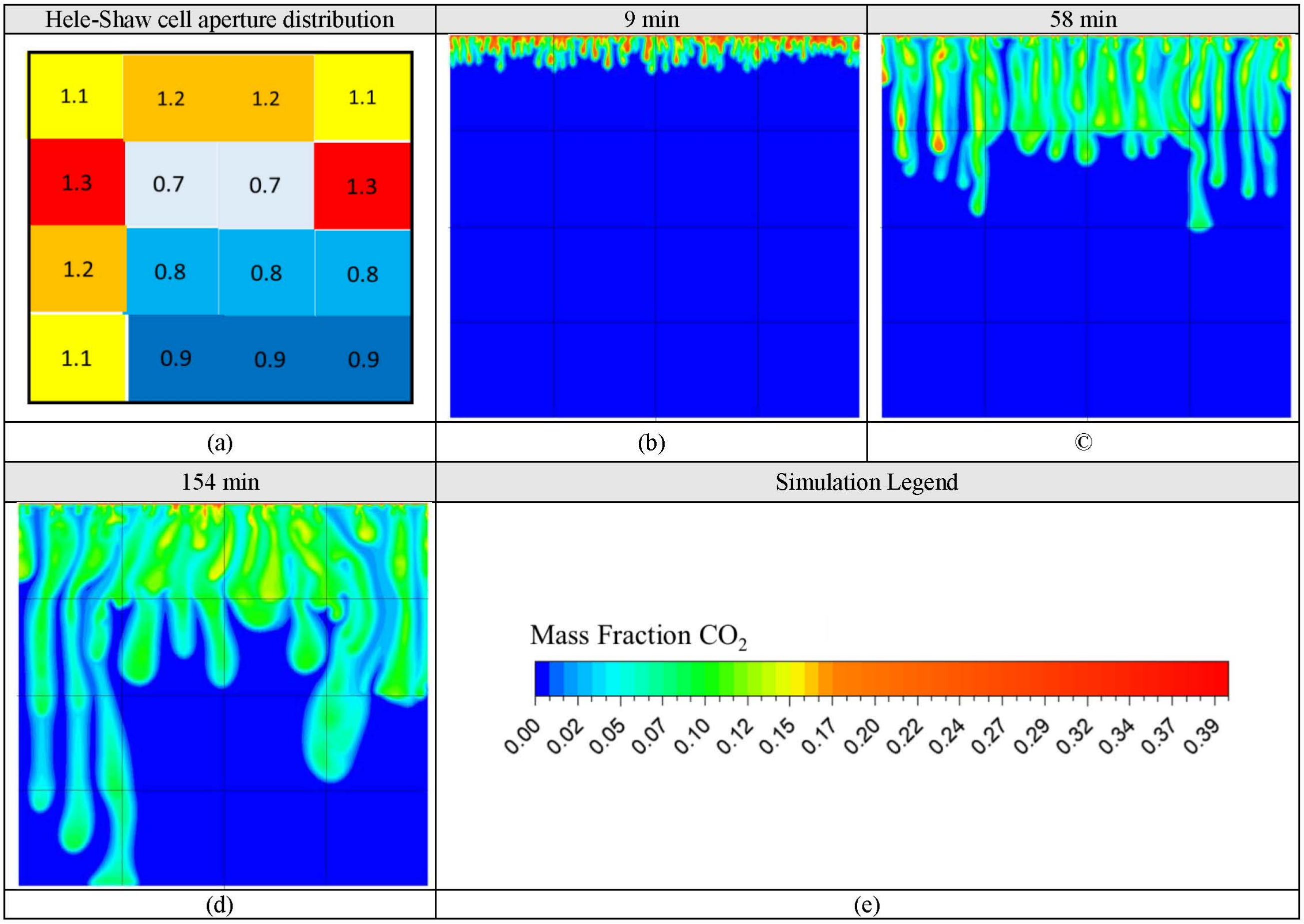

Figure 3—(a) Hele-Shaw cell aperture distribution (expressed in millimeters) and (b-d) the evolution of CO_2 dissolution through time for heterogeneous Case 2. The mass fraction of CO_2 is shown in (e)

Results and Discussions

As shown in Fig. 2, the permeability distribution is set to be in a certain manner so that a high permeability region follows a low permeability one, all while keeping the average permeability to be 8.33×10^{-8} (Hele-Shaw cell aperture of 1 mm). Although the initial stages of the CO_2 dissolution are similar to the homogeneous case, the tip of the CO_2 dissolved finger-shaped regions exhibits a preferential flow towards the high permeable regions, clearly observable on the second row at 58 minutes (Fig. 2c). Similar preferential movement is also observed in our previous study (Shahriar & Khanal, 2023b). Furthermore, this vertical finger travel is also high in high permeability regions. Compared to the homogeneous case (Fig. 1), heterogeneous case 1 has lower vertical travel at the end of the simulation (154 minutes). Furthermore, at the end of the simulation period, it is found that more CO_2 is dissolved in the homogeneous case by comparing the average CO_2 concentration for the homogeneous case (5.797×10^{-4} mol/L) and heterogeneous case 1 (5.787×10^{-4} mol/L). (Taheri et al., 2018) also observed higher cumulative CO_2 dissolved in homogenous conditions than in heterogeneous cases. This shows that reservoirs with no or low permeability heterogeneity are preferable for higher CO_2 dissolution.

Although the heterogeneous case 1 has permeability variation, the overall CO_2 dissolved region seems to move downwards uniformly. This can be attributed to the effects of low connectivity between the high permeability zones, preventing the formation of any particular preferential flow region. However, the effect of connectivity in creating preferential flow regions is observable in heterogeneous case 2 (Fig. 3), where the high permeability regions are stacked vertically, and the low permeability regions are placed together in the bottom right corner of the cell, as observed in the aperture distribution, shown in Fig. 3a.

As shown in Fig. 3, the CO_2 dissolved region follows a preferential path and an uneven CO_2 sweep in the low permeability regions. This channeling effect can be attributed to the good connectivity between the high permeability zones. Another interesting phenomenon is observed in the heterogeneous case 2; although faster vertical travel is exhibited in the high permeability zones (CO_2 dissolved region reaches the bottom of the cell in about 154 minutes), the overall CO_2 dissolution in heterogeneity case 2 is the lowest with average CO_2 concentration of 5.769×10^{-4} mol/L, compared to the homogeneous case (5.797×10^{-4} mol/L) and heterogeneous case 1 (5.787×10^{-4} mol/L). The lower CO_2 dissolution in this scenario can be attributed to the poor CO_2 dissolution in the low permeability regions. Since all the cases considered in the study have similar average permeability, it is safe to assume that the permeability distribution in different regions can lead to faster or slower CO_2 storage, also dictated by the connectivity of the permeability zones.

Although this study considers the effect of permeability distribution for an average permeability corresponding to a cell aperture of 1 mm, i.e., fluid flow in the Darcy regime based on the numerical considerations, future studies can consider both Hele-Shaw and 3D flow regimes for CO_2 dissolution in heterogeneous media. Another factor worth noting is that although this study considers fluid flow in the Darcy regime, where the effect of gap-induced dispersion is negligible, future studies can incorporate 3D models to report any change in dissolution behavior (Shahriar & Khanal, 2023b). Further insights into the effect of permeability distribution are obtainable through multiple variations of the heterogeneity cases and will be considered in future studies.

Conclusions

This study explored the CO_2 dissolution behavior due to permeability distribution using two heterogeneous cases with the same average permeability and compared them with the homogeneous case. Nonuniform finger movement is observed due to spatial permeability heterogeneity, where alongside faster vertical travel, the preferential finger movement is towards the high permeability zones. Furthermore, the simulation results highlighted the uneven CO_2 concentration inside the convective fingers. The average CO_2 concentration after 154 minutes follows the order of homogenous case (5.797×10^{-4} mol/L) > heterogeneous case 1 (5.787×10^{-4} mol/L) > heterogeneous case 2 (5.769×10^{-4} mol/L), illustrating the importance of considering connectivity channels and permeability distribution during CO_2 dissolution. The preferential flow path is more prominent in heterogeneous cases with high connectivity. The proposed methodology in this study can also be extended to analyze more complex heterogeneous systems for different fluid flow regimes. The findings of this study will add to the existing knowledge on the effect of permeability distribution in CO_2 dissolution in saline aquifers.

Acknowledgments

This research was partially funded by the National Science Foundation Award under CBET-2245484U.S and the Department of Energy Office of Science, Basic Energy Sciences' Geoscience program under Award Number DE-SC0024642. Any opinions, findings, conclusions or recommendations expressed in this material are those of the author(s) and do not necessarily reflect the views of the funding agencies.

References

Aldred, F., Gobron, N., Miller, J. B., Willett, K. M., & Dunn, R. (2021). Global climate. *Bulletin of the American Meteorological Society*, **102**(8), S11–S142. https://doi.org/10.1175/BAMS-D-21-0098.1

Alipour, M., De Paoli, M., & Soldati, A. (2020). Concentration-based velocity reconstruction in convective Hele–Shaw flows. *Experiments in Fluids*, **61**(9). https://doi.org/10.1007/s00348-020-03016-3

Amarasinghe, W., Fjelde, I., Rydland, J. Å., & Guo, Y. (2020). Effects of permeability on CO2 dissolution and convection at reservoir temperature and pressure conditions: A visualization study. *International Journal of Greenhouse Gas Control*, **99**(November 2019). https://doi.org/10.1016/j.ijggc.2020.103082

Amarasinghe, W. S., Fjelde, I., & Flaata, A. M. N. (2021). Visual investigation of CO2 dissolution and convection in heterogeneous porous media at reservoir temperature and pressure conditions. *Greenhouse Gases: Science and Technology*, **11**(2), 342–359. https://doi.org/10.1002/ghg.2055

Chevalier, S., Faisal, T. F., Bernabe, Y., Juanes, R., & Sassi, M. (2015). Numerical sensitivity analysis of density driven CO2 convection with respect to different modeling and boundary conditions. *Heat and Mass Transfer/Waerme- Und Stoffuebertragung*, **51**(7), 941–952. https://doi.org/10.1007/s00231-014-1466-2

De, N., Singh, N., Fulcrand, R., Méheust, Y., Meunier, P., & Nadal, F. (2022). Two-dimensional micromodels for studying the convective dissolution of carbon dioxide in 2D water-saturated porous media. *Lab on a Chip*, **22**(23), 4645–4655. https://doi.org/10.1039/D2LC00540A

De Paoli, M., Alipour, M., & Soldati, A. (2020). How non-Darcy effects influence scaling laws in Hele-Shaw convection experiments. *Journal of Fluid Mechanics*. https://doi.org/10.1017/jfm.2020.229

Emami-Meybodi, H., Hassanzadeh, H., Green, C. P., & Ennis-King, J. (2015). Convective dissolution of CO2 in saline aquifers: Progress in modeling and experiments. *International Journal of Greenhouse Gas Control*, **40**, 238–266. https://doi.org/10.1016/j.ijggc.2015.04.003

Faisal, T. F., Chevalier, S., Bernabe, Y., Juanes, R., & Sassi, M. (2015). Quantitative and qualitative study of density driven CO2 mass transfer in a vertical Hele-Shaw cell. *International Journal of Heat and Mass Transfer*, **81**, 901–914. https://doi.org/10.1016/j.ijheatmasstransfer.2014.11.017

Farajzadeh, R., Farshbaf Zinati, F., Zitha, P. L. J., & Bruining, J. (2008). Density-driven natural convection in dual layered and anisotropic porous media with application for CO2 injection project. ECMOR 2008 - 11th European Conference on the Mathematics of Oil Recovery. https://doi.org/10.3997/2214-4609.20146391

Farajzadeh, R., Ranganathan, P., Zitha, P. L. J., Bruining, J., Farajzadeh, R., Ranganathan, P., Zitha, P. L. J., & Bruining, J. (2011). The effect of heterogeneity on the character of density-driven natural convection of CO2 overlying a brine layer. *Advances in Water Resources*, **34**(3), 327–339. https://doi.org/10.1016/j.advwatres.2010.12.012

Ferziger, J. H., Perić, M., & Street, R. L. (2020). Computational Methods for Fluid Dynamics. In *Computational Methods for Fluid Dynamics*. https://doi.org/10.1007/978-3-319-99693-6

Khanal, A., & Shahriar, M. F. (2022). Physics-Based Proxy Modeling of CO2 Sequestration in Deep Saline Aquifers. *Energies*, **15**(12), 4350. https://doi.org/10.3390/en15124350

Khosrokhavar, R., Elsinga, G., Farajzadeh, R., & Bruining, H. (2014). Visualization and investigation of natural convection flow of CO2 in aqueous and oleic systems. *Journal of Petroleum Science and Engineering*, **122**, 230–239. https://doi.org/10.1016/j.petrol.2014.07.016

Kneafsey, T. J., & Pruess, K. (2010). Laboratory flow experiments for visualizing carbon dioxide-induced, density-driven brine convection. *Transport in Porous Media*, **82**(1), 123–139. https://doi.org/10.1007/s11242-009-9482-2

Mahmoodpour, S., Rostami, B., Soltanian, M. R., & Amooie, M. A. (2019). Convective Dissolution of Carbon Dioxide in Deep Saline Aquifers: Insights from Engineering a High-Pressure Porous Visual Cell. *Physical Review Applied*, **12**(3). https://doi.org/10.1103/PhysRevApplied.12.034016

Mahyapour, R., Mahmoodpour, S., Singh, M., & Omrani, S. (2022). Effect of permeability heterogeneity on the dissolution process during carbon dioxide sequestration in saline aquifers: two-and three-dimensional structures. *Geomechanics and Geophysics for Geo-Energy and Geo-Resources*, **8**(2). https://doi.org/10.1007/s40948-022-00377-3

Outeda, R., El Hasi, C., D'Onofrio, A., & Zalts, A. (2014). Experimental study of linear and nonlinear regimes of density-driven instabilities induced by CO(2) dissolution in water. *Chaos (Woodbury, N.Y.)*, **24**(1), 013135. https://doi.org/10.1063/1.4868040

Shahriar, M. F., & Khanal, A. (2023a). Fundamental investigation of reactive-convective transport: Implications for long-term carbon dioxide (CO2) sequestration. *International Journal of Greenhouse Gas Control*, **127**, 103916. https://doi.org/10.1016/j.ijggc.2023.103916

Shahriar, M. F., & Khanal, A. (2023b). Effect of Formation Heterogeneity on CO 2 Dissolution in Subsurface Porous Media. *ACS Earth and Space Chemistry*. https://doi.org/10.1021/acsearthspacechem.3c00175

Singh, A., Singh, Y., & Pandey, K. M. (2019). Viscous fingering instabilities in radial Hele-Shaw cell: A review. Materials Today: Proceedings, **26**, 760–762. https://doi.org/10.1016/j.matpr.2020.01.022

Soboleva, E. B. (2018). Density-driven convection in an inhomogeneous geothermal reservoir. *International Journal of Heat and Mass Transfer*, **127**, 784–798. https://doi.org/10.1016/j.ijheatmasstransfer.2018.08.019

Soltanian, M. R., Amooie, M. A., Gershenzon, N., Dai, Z., Ritzi, R., Xiong, F., Cole, D., & Moortgat, J. (2017). Dissolution Trapping of Carbon Dioxide in Heterogeneous Aquifers. *Environmental Science and Technology*, **51**(13), 7732–7741. https://doi.org/10.1021/acs.est.7b01540

Taheri, A., Lindeberg, E., Torsæter, O., & Wessel-Berg, D. (2017). Qualitative and quantitative experimental study of convective mixing process during storage of CO2 in homogeneous saline aquifers. *International Journal of Greenhouse Gas Control*, **66**(August), 159–176. https://doi.org/10.1016/j.ijggc.2017.08.023

Taheri, A., Torsæter, O., Lindeberg, E., Hadia, N. J., & Wessel-Berg, D. (2018). Qualitative and quantitative experimental study of convective mixing process during storage of CO2 in heterogeneous saline aquifers. *International Journal of Greenhouse Gas Control*, **71**(October 2016), 212–226. https://doi.org/10.1016/j.ijggc.2018.02.003

Vosper, H., Kirk, K., Rochelle, C., Noy, D., & Chadwick, A. (2014). Does numerical modelling of the onset of dissolution-convection reliably reproduce this key stabilization process in CO2 Storage? *Energy Procedia*, **63**, 5341–5348. https://doi.org/10.1016/j.egypro.2014.11.566

Wang, Y.-Y., Wang, X.-G., Dong, R.-C., Teng, W.-C., Zhan, S.-Y., Zeng, G.-Y., & Jia, C.-Q. (2023). Reservoir heterogeneity controls of CO2-EOR and storage potentials in residual oil zones: Insights from numerical simulations. *Petroleum Science*. https://doi.org/10.1016/j.petsci.2023.03.023

Zhang, Z., Fu, Q., Zhang, H., Yuan, X., & Yu, K. T. (2020). Experimental and Numerical Investigation on Interfacial Mass Transfer Mechanism for Rayleigh Convection in Hele-Shaw Cell. *Industrial and Engineering Chemistry Research*, **59**(21), 10195–10209. https://doi.org/10.1021/acs.iecr.0c01345